Journal of Hepatocellular Carcinoma

Dovepress
Taylor & Francis Group

Open Access Full Text Article

ORIGINAL RESEARCH

Design and Mechanism Study of 6c, a Novel Artesunate Derivatives, for Anti-Hepatocellular Carcinoma

Shang-Shang Xiong

Departments of Pharmacology, School of Pharmacy, Qingdao University Medical College, Shandong, People's Republic of China

Correspondence: Shang-Shang Xiong, Email 17355138325@163.com

Objective: Artesunate can inhibit the proliferation of various tumor cells and has practical value in developing anti-tumor drugs. However, its biological activity against hepatocellular carcinoma is weak. The efficacy of its anti-tumor effect needs to be improved.
Methods: 11 compounds of three types were designed and synthesized. Their antitumor activity was detected by MTT assay in vitro and subcutaneous xenograft model in vivo. Then, DCFH-DA probe detection and NAC intervention experiments were used to detect ROS levels. The ferroptosis inhibitor (Liproxstatin-1) was used to study the effect of compound 6c in inducing ferroptosis. Western blot was used to observe the expression of apoptosis-related proteins. The ability of 6c to induce apoptosis was detected by Annexin V-FITC/PI double staining and Hoechst 33342 staining experiment. The effect of 6c on cycle arrest was detected by flow cytometry. Molecular simulations of several hybrids with vascular endothelial growth factor receptor 2 (*VEGFR-2*) and Transferrin receptor protein 1 (*TFR1*) were performed using MOE molecular docking software.
Results: A series of new artemisinin-4-(4-substituted phenoxy) pyridine derivatives were synthesized and their anticancer activities were tested in three lines of hepatocellular carcinoma (HCC) cells. Among the hybrid hits with anticancer activity, a representative 6c compound increased the reactive oxygen species (ROS) level in hepatocellular carcinoma cells and activated mitochondrial apoptosis and ferroptosis, leading to cell cycle arrest at G2/M phase. Molecular docking shows the binding of 6c compound to oncogenic vascular endothelial growth factor receptor 2 (*VEGFR-2*) and Transferrin receptor protein 1 (*TFR1*) that are overexpressed in malignant epithelial tumors.
Conclusion: Taken together, our identification of the promising compound 6c may hold developmental potential for therapy of hepatocellular carcinoma.

Keywords: hepatocellular carcinoma, artesunate, phenoxy-pyridine, hybridization, reactive oxygen species, apoptosis, docking

Introduction

Hepatocellular carcinoma (HCC) has been ranked as the seventh most common cancer in the world, with more than 20 million new cases and more than 9.7 million in 2022.[1] Currently, the common molecular targeted drugs for treating HCC on the market, such as sorafenib and regorafenib, are difficult to improve the 5-year survival rate of patients.[2] These drugs have some obvious disadvantages, such as limited efficacy, significant toxic side effects, and lack of selectivity. Therefore, it is urgent to find new and more effective anti-HCC drugs. Modifying existing clinical anti-HCC drugs is one of the feasible methods to find new chemotherapy candidate drugs.

Artesunate is a water-soluble derivative of artemisinin, a monomer isolated from the traditional Chinese medicinal herb plant *Artemisia annua* for effective treatment of malaria with very low host toxicity (Figure 1).[3] Artesunate is the first-line drug for treating severe malaria in children or adults.[4] Compared with artemisinin, artesunate has better biological activity, absorption, solubility, and pharmacokinetic characteristics[5,6] (Figure S1). Numerous studies have shown that artesunate is effective against malaria and has anti-tumor activity.[7] Considerable in vitro and in vivo studies have shown that artesunate and its derivatives exhibit therapeutic potential against cancer with radio sensitizing effect, less drug resistance and also low toxicity to normal cells.[8–10] It is reported that the 1,2,4-trioxane moiety of artesunate is

Received: 10 October 2024
Accepted: 17 January 2025
Published: 25 January 2025

Graphical Abstract

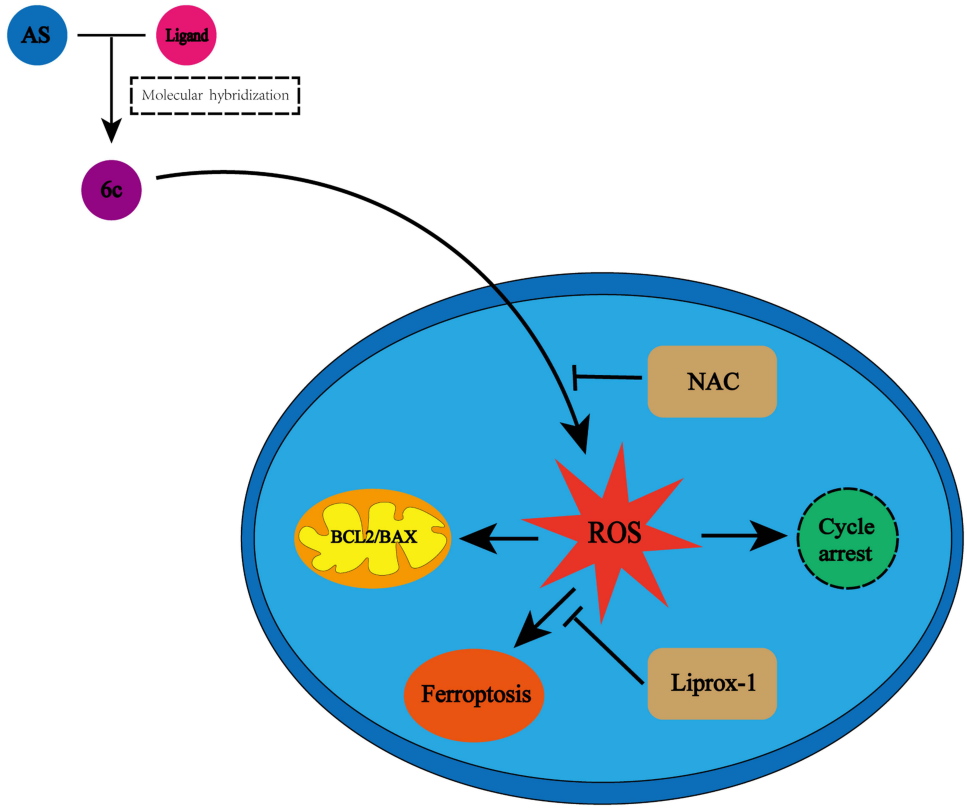

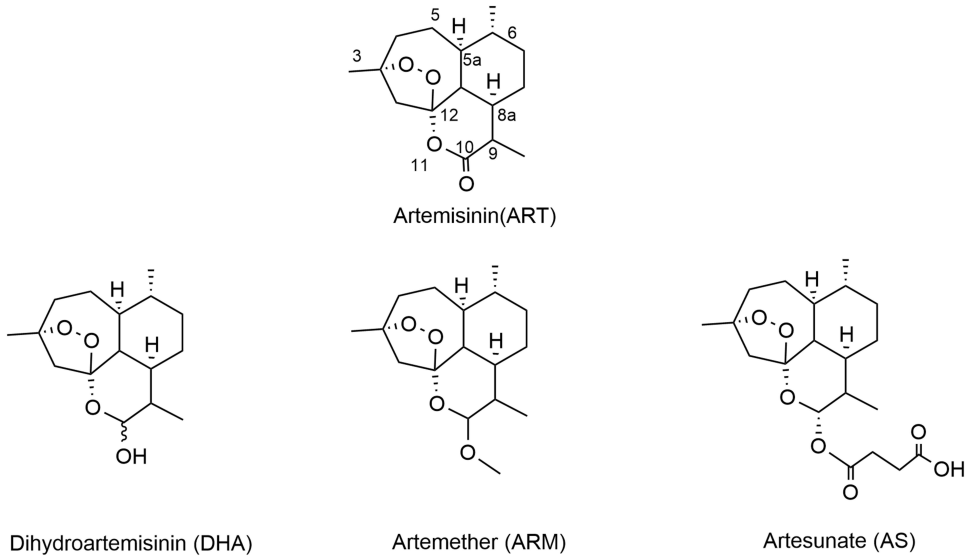

Figure 1 Artesunate and its derivatives.

critical in generating reactive oxygen species (ROS) by cleaving peroxide bridges,[11–14] and the accumulation of ROS induces apoptosis, ferroptosis, autophagy, and other programmed death pathways.[15–18] These observations suggest that chemical modifications of artesunate may improve its anti-tumor activity with less toxicity.

Molecular hybridization serves as a medicinal chemistry strategy that combines two active pharmacophore groups through linkers for generation of novel hybrid compounds for improvement of bioactivity.[19–22] It has been shown that introduction of 4-(arylamino) quinazoline pharmacophore to artemisinin skeleton through different linkers can generate artemisinin analogs with robust antiproliferative activities against human colorectal cancer cells, melanoma cells and inhibition of xenograft tumor growth.[19] Combination of artesunate with sorafenib, artesunate can also synergistically increase the antitumor activity of sorafenib and reverse the resistance of tumors to sorafenib.[23–25] These observations suggest that combining two distinct chemical entities may lead to synergistic improvement in their activity with reduced side effects of both compounds.

In this study, we utilized the molecular hybridization approach by combining the artesunate 1,2,4-trioxane group critical for anti-tumor activity with the core pharmacophore of tyrosine kinase inhibitors gefitinib and sorafenib. Here, we report the synthesis of a series of artesunate hybrids using phenyl-substituted pyridines as linker. The biological activity of these hybrid compounds was tested in Hep3B, HepG2, and Huh7 cells as well as the cytotoxicity in human normal liver cells (LO2). A representative compound 6c exhibits robust anti-HCC activity and low cytotoxicity to normal cells. Mechanistically, 6c causes an increased level of intracellular reactive oxygen species and induces cell ferroptosis, cell cycle arrest, and apoptosis.

Results

Chemistry

Synthesis of Artesunate Hybrids with 5-Substituted Phenylpyridine Linker

We initiated the synthesis of the first series of artesunate hybrids 6a-e featured with 5-substituted phenylpyridine linkers from starting 4-(4-aminophenoxy)-N-methyl-2-pyridinecarboxamide 1 and 5-bromopicolinic acid 2 for generation of compound 3 by amide bond-forming reaction catalyzed by oxalyl chloride. Subsequently, compounds 5a-e were synthesized from compound 3 and phenylboronic acid 4a-e by Suzuki coupling reaction using bis (triphenylphosphine) palladium(II) dichloride as a catalyst under alkaline conditions in water and 1,4-dioxane with a strong yield. In the presence of EDCl and DMAP, artesunate (AS) 7 is combined with alcohol 5a-e to produce 6a-e, respectively (Scheme 1).

Synthesis of Artesunate Hybrids with 4-Substituted Phenylpyridine Linker

4-(4-aminophenoxy)-n-methyl-2-pyridinecarboxylic acid 1 and 4-bromoquinolinic acid 8 were converted to compound 9 through an acylation reaction under the catalysis of oxalyl chloride. Compound 9 took place via Suzuki coupling reaction with corresponding phenylboronic acid 4a-e to generate compounds 10a-e under alkaline conditions in water and

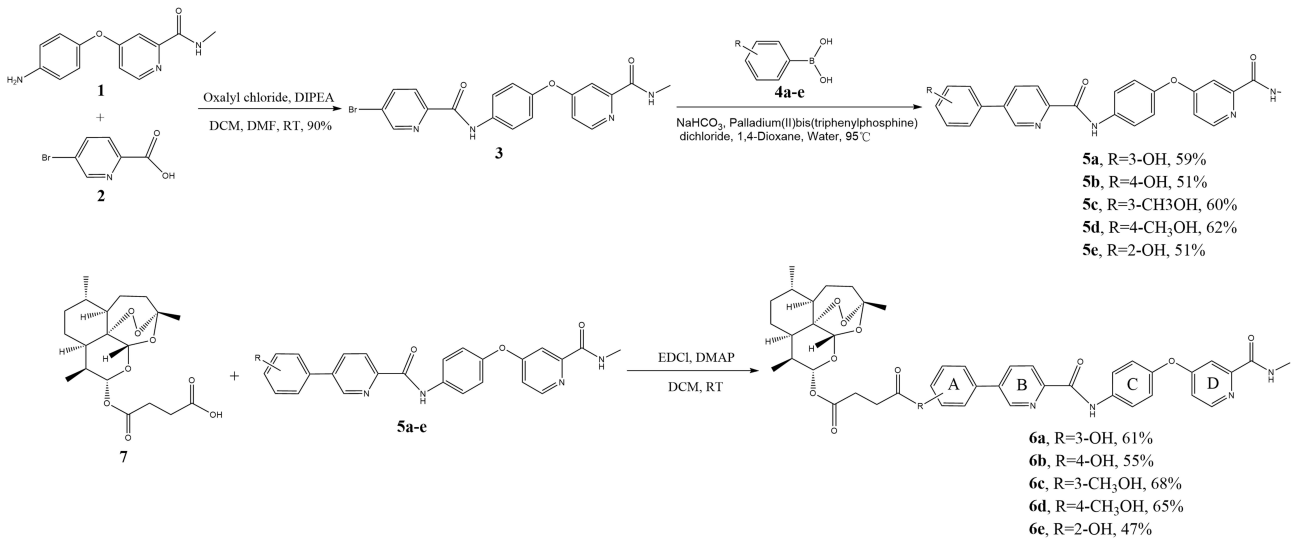

Scheme 1 Synthesis of artesunate hybrids with 5-substituted phenylpyridine linker.

https://doi.org/10.2147/JHC.S490445

1,4-dioxane with a high yield. Artesunate (AS) 7 coupled with compounds 10a-e led to generation of compounds 11a-e, respectively (Scheme 2).

Synthesis of Artesunate Hybrid with No Linker

Artesunate hybrid 12 was synthesized by the amidation reaction of artesunate (AS) 7 and 4-(4-amino phenoxy)-N-methyl-2-pyridinecarboxylic acid amide 1 under the catalysis of EDCl, DMAP, and HoBt (Scheme 3).

Pharmacology

In vitro Anti-HCC Activity

We tested the effect of synthesized hybrids on cell viability of human hepatocellular carcinoma cells from three cell lines of HepG2, Hep3B, Huh7, and also a human normal liver cell line LO2 in MTT assay. We started evaluating the effects of 5-substituted phenylpyridine linkers (6a-e) at different substitution positions of the benzene ring (A) on HepG2, Hep3B, Huh7, and LO2 cells. Compounds 6a and 6c showed potent anti-proliferative effects on three hepatocellular carcinoma (HCC) cell lines with their IC_{50} values about 10–20 times smaller than lead compound artesunate (Table 1), which is equivalent to the IC_{50} of Sorafenib, a clinically positive drug for the treatment of hepatocellular carcinoma. The cytotoxicity of 6c was 12 times less than that of sorafenib on human normal liver cells LO2 and 2 times less than artesunate (AS). As far as the preliminary structure-activity relationship is concerned, the activity of compounds in which the phenolic hydroxyl group was substituted to the meta of the benzene ring (A) showed higher than para or ortho which

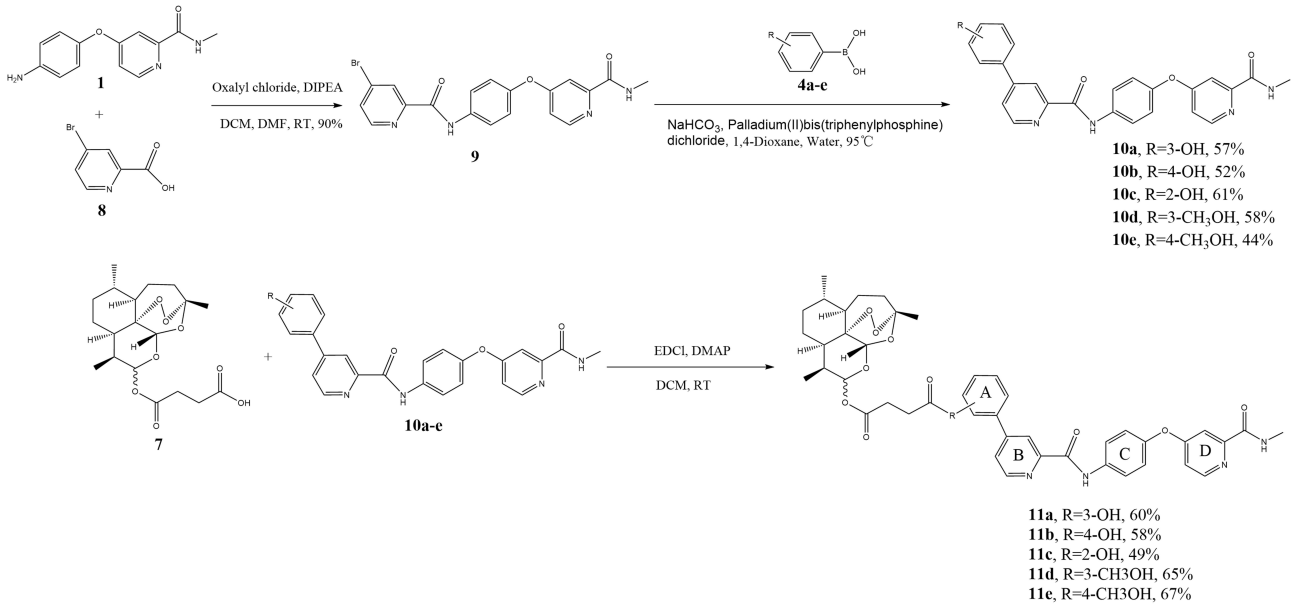

Scheme 2 Synthesis of artesunate hybrids with 4-substituted phenylpyridine linker.

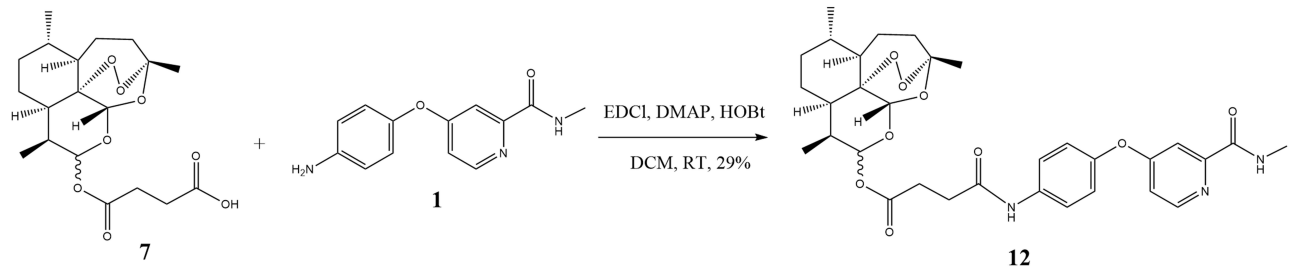

Scheme 3 Synthesis of artesunate hybrid with no linker.

 https://doi.org/10.2147/JHC.S490445

Table 1 The IC_{50} Values of Artesunate derivatives Against Human Hepatocarcinoma Cell Lines and Selectivity Index

Compound	R	IC_{50} (μM)[a]				Selectivity Index		
		HepG2	Huh7	Hep3B	LO2[b]	SI 1[d]	SI 2[e]	SI 3[f]
6a	3-OH	4.49±0.26	1.65±0.16	4.06±0.24	30.65±2.55	6.8	18.6	7.5
6b	4-OH	8.33±0.18	3.18±0.23	7.28±0.51	45.97±3.53	5.5	14.5	6.3
6c	3-CH3OH	8.5±0.98	2.25±0.21	5.35±0.57	>100	>11.8	>44.4	>18.7
6d	4-CH3OH	11.14±0.77	7.79±2.39	9.88±0.32	>100	>8.9	>12.8	>10.1
6e	2-OH	16.28±1.3	5.83±0.51	8.67±0.69	>100	>6.1	>17.1	>11.5
11a	3-OH	12.28±1.17	7.97±0.42	8.20±0.31	44.05±3.23	3.6	5.5	5.3
11b	4-OH	15.31±1.44	12.22±1.07	6.19±1.85	37.75±1.16	2.5	3.1	6.1
11c	2-OH	7.23±0.74	4.35±0.38	6.15±0.41	42.70±3.57	5.9	9.8	6.9
11d	3-CH3OH	9.93±0.77	10.78±0.95	8.73±0.75	64.47±3.57	6.5	5.9	7.4
11e	4-CH3OH	19.16±1.61	12.79±0.85	10.87±1.03	48.08±1.27	2.5	3.8	4.4
12	–	NT[c]	12.64±1.52	24.55±1.89	50.8±1.48	ND[g]	4	2.1
1	–	NT[c]	>100	>100	NT[c]	ND[g]	ND[g]	ND[g]
AS	–	42.82±1.44	47.54±1.39	44.17±2.16	72.31±1.37	1.7	1.5	1.6
Sorafenib	–	6.45±0.32	3.09±0.08	4.33±0.36	8.63±0.12	1.3	2.8	2

Notes: [a]The IC $_{50}$ values were calculated from three independent experiments and represented the mean ±SD (n= 3). The incubation time of cells was 72h. [b] LO2 cell line of normal human hepatocytes. [c] NT: not tested. [d] SI1 = IC_{50} LO_2/IC_{50} HepG2. [e] SI2 = IC_{50} LO_2/IC_{50} Huh7. [f] SI3 = IC_{50} LO_2/IC_{50} Hep3B. [g] ND: not determined.

had the worst activity. The activity of hybrids that were linked via phenolic hydroxyl with carboxylic acid is higher than that of hybrids linked by benzyl alcohol with carboxylic acid. But in this case, these hybrids exerted tiny differences in the bioactivities. However, for normal cells, LO2, the cytotoxicity of the latter is much lower than that of the former, and the cytotoxicity of hybrids linked to the 2-position of the benzene ring (A) is inferior to that of 3-position and 4-position hybrids.

The activities of hybrids (11a-e) with the 4-substituted phenylpyridine linker were also evaluated on the three cancer cell lines, and its overall activity was not as good as that of the hybrids with the 5-substituted phenylpyridine linker. Interestingly, in contrast to the hybrids using 5-substituted phenylpyridine linkers, the activities of the hybrids forming ester bond via benzyl alcohol groups in 11d-e were lower than that through phenolic hydroxyl groups (11a-c). The activity of the hybrids substituted at ortho was higher than that of the hybrids substituted at meta and para on the benzene ring (A). There was little difference in the cytotoxicity of these hybrids in normal cell line LO2.

When no linker was used, the anti-proliferation ability of the hybrid (12) against hepatocellular carcinoma cells was significantly reduced as compared to the previous hybrids 6a-e and 11a-e with phenylpyridine linkers. Its cytotoxicity was almost the same as its precursor compound artesunate. In addition, artesunate or compound 1 (4-(aminophenoxy)-N-methylpicolinamide) showed weak biological activity in these cancer cell lines, and the hybrids with 5-substituted phenylpyridine linker exhibited the best biological activity.

Compound Selection Index

We further analyzed the selection index of these series of hybrids against normal liver cells over hepatocellular carcinoma cells. As shown in Table 1, the series of hybrids achieved a relatively excellent selection index, as compared to artesunate (AS) or sorafenib. Among them, 6c had the highest selection index, indicating that the cytotoxicity of compound 6c to cancer cells is greater than normal cells.

Concentration- and Time-Dependent Inhibition of Hepatocellular Carcinoma Proliferation by Compound 6c

We further tested the concentration- and time-dependent effect of a promising compound 6c on proliferation of Hep3B and Huh7 cells using MTT assay. We treated the cells with a series concentration of 6c and 24 h, 48 h, and 72 h. Cell Viability decreased with concentration and time (Figure 2A and B). These results indicated that 6c inhibit HCC cells growth with a time- and concentration-dependent manner.

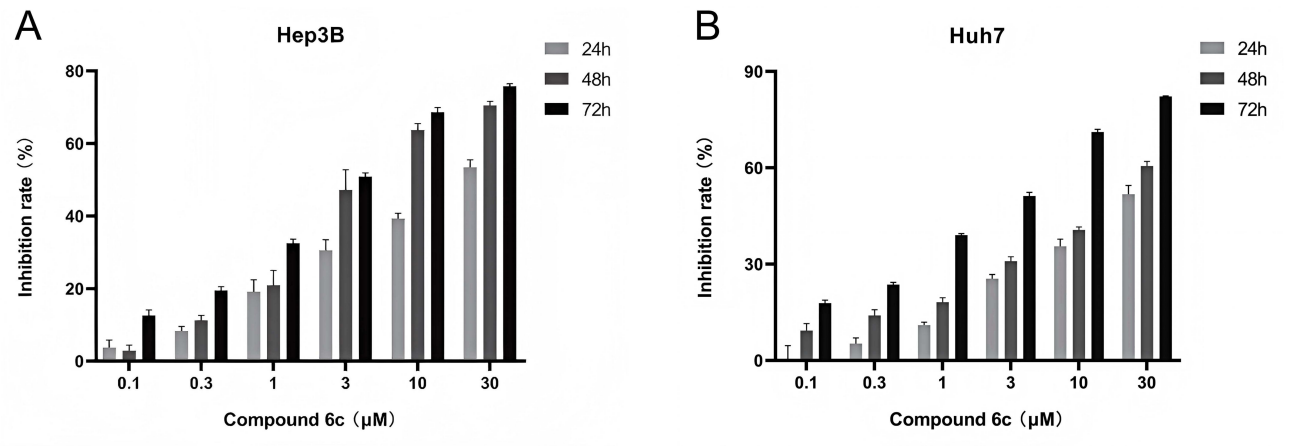

Figure 2 Compound 6c inhibits the proliferation of hepatocellular carcinoma cells in MTT assay. (**A**) Hep3B and (**B**) Huh7 cells were treated with 6c for 24, 48h, 72h. The compound 6c inhibited cell proliferation in a concentration-dependent and time-dependent manner (n=3).

Compound 6c Exerts Anti-Proliferation Effect in HCC via ROS

As compound 6c is a derivative of artemisinin, we hypothesize that 6c may also exert its anti-tumor effect by regulating ROS levels in tumor cells. To verify the hypothesis that 6c can induce reactive oxygen species generated in HCC, we treated the cells with 6c at 5 μM, 10 μM, and 20 μM for 4 h and detected the intracellular reactive oxygen species content using a DCFH-DA probe. The results are shown in Figure 3A and B, where 6c induced the production of reactive oxygen species with a concentration-dependent manner. Then, we used N-acetylcysteine (NAC), which is an antioxidant with cell membrane permeability and can reduce the level of reactive oxygen species. Huh7 and Hep3B cells were co-treated with 5 or 10 mm N-acetylcysteine and 10 μM 6c for 24, 48, and 72 h. As shown in Figure 3C–E, inhibition of ROS production by N-acetylcysteine reversed the inhibitory effect of 6c on proliferation of Huh7 cells in time- and concentration-dependent manner. These results demonstrate that the level of reactive oxygen species is critical for 6c-mediated anti-HCC proliferation.

Compound 6c Induced Ferroptosis in HCC

Ferroptosis is a novel discovered pathway of cell death. Studies have shown that iron-dependent accumulation of reactive oxygen species (ROS) may trigger cell death in the form of ferroptosis.[26] It has been previously demonstrated that compound 6c exerts its anti-HCC effect through reactive oxygen species (ROS). Therefore, we hypothesized that 6c might exert its effect by inducing ferroptosis in HCC. As shown in Figure 4A, Huh7 cells were pretreated with 6c for 24h, 48h, and 72h, and treated with the ferroptosis inhibitor Liproxstatin-1, which had the effect of reversing cell death. As shown in Figure 4B, during treatment of Huh7 cells with 10 μM compound 6c for 72 h, Liproxstatin-1 reversed cell death in a concentration-dependent manner. These results demonstrate that hybrid 6c induces ferroptosis in Huh7 cells.

Compound 6c Activates the Mitochondrial Apoptosis Pathway

A high level of reactive oxygen species (ROS) is known to suppress tumor growth through activation of apoptosis.[27] We examined the effect of 6c on expressions of Bax and Bcl-2 proteins in Huh7 cells. As shown in Figure 5A, the expression of Bax protein in Huh7 cells was increased in response to increasing concentrations of 6c, whereas the expression of Bcl-2 protein was decreased. As a result, the ratio of Bcl-2/Bax was concentration-dependently decreased in response to treatment of different concentrations of compound 6c for 48 h (Figure 5B). These results demonstrate that 6c induces the activation of mitochondrial apoptotic pathway in Huh7 cells.

Induction of Cell Apoptosis by Compound 6c

7To further examine whether the anti-tumor activity of compound 6c is related to cell apoptosis, early apoptosis was measured by Annexin V-FITC assay. The cells were collected and stained with apoptosis kit and analyzed by flow cytometry after cells

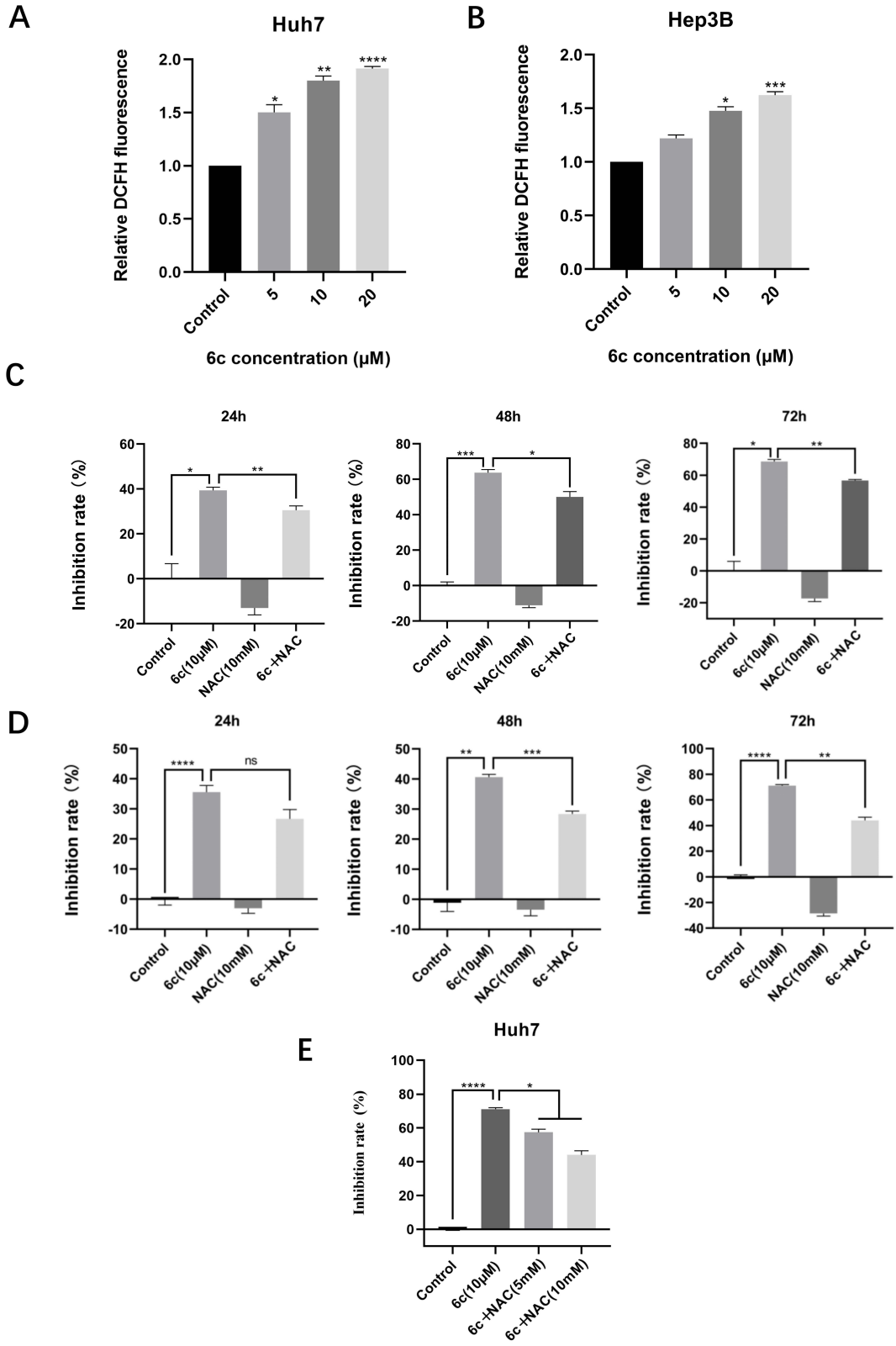

Figure 3 Inhibition of proliferation of HCC cells by compound 6c via ROS. (**A**) Huh7 cells and (**B**) Hep3B cells were treated with 6c for 4h. (**C**) Huh7 cells and (**D**) Hep3B cells were treated with 6c alone or plus N-acetyl-L-cysteine (NAC) for 24, 48h, and 72 h. (**E**) Cells were co-treated with different concentrations of NAC and 10 μM 6c cultured for 72 h. **P* <0.05; ***P* <0.01; ****P* <0.001; *****P* <0.0001.

Abbreviations: ns, not significant.

https://doi.org/10.2147/JHC.S490445

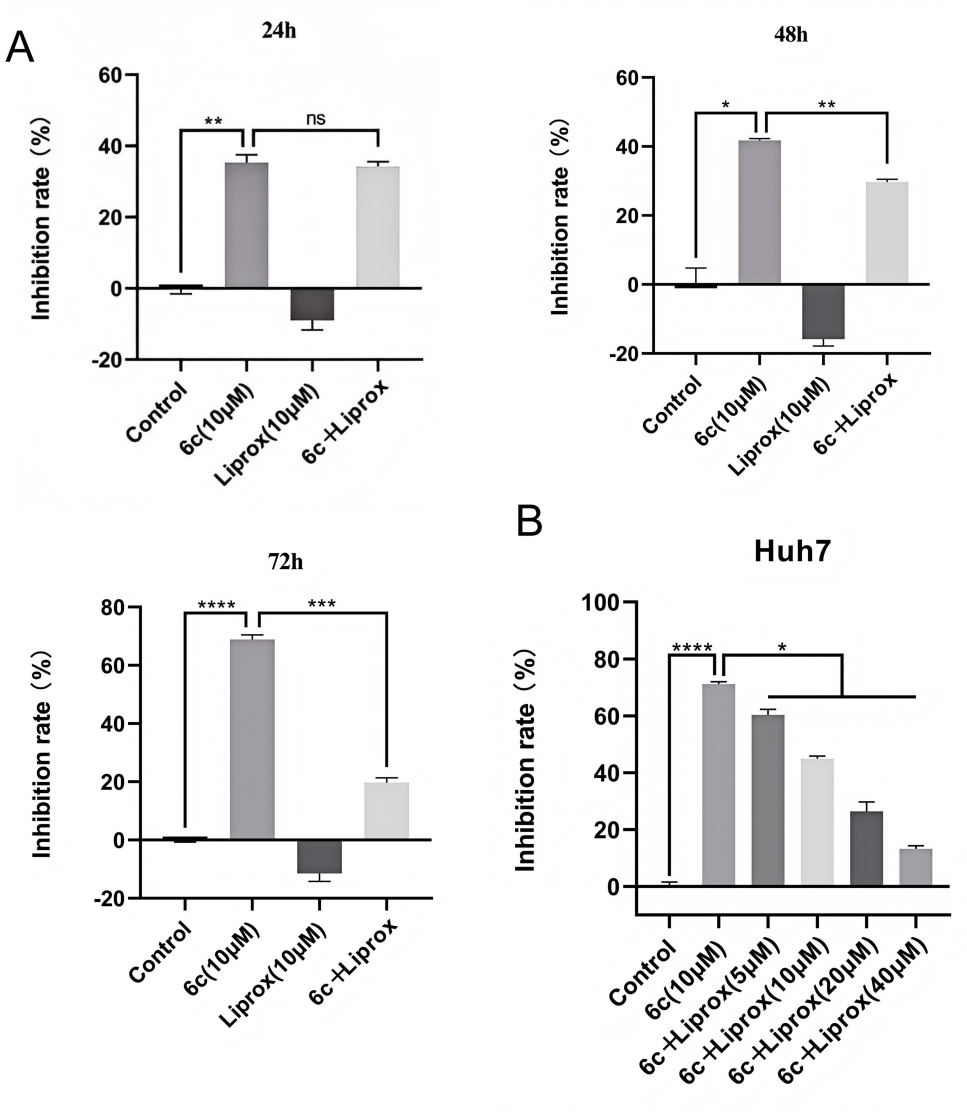

Figure 4 Induction of ferroptosis in Huh7 cells by compound 6c. (**A**) Huh7 cells were treated with 6c alone or plus Liproxstatin-1 for 24, 48h, and 72 h. (**B**) Cells were co-treated with different concentrations of Liproxstatin-1 and 10 μM 6c cultured for 72 h. *P <0.05; **P <0.01; ***P <0.001; ****P <0.0001.
Abbreviations: ns, not significant.

were treated with different concentrations of 6c for 24 h. As shown in Figure 6A and B, the percentages of apoptotic cells were 6.9%, 9.2%, 17.2%, 18.7%, and 24.2%, which were higher than the control group (4.9%), suggesting that 6c induces cell apoptosis in a concentration-dependent manner. To further verify that 6c causes apoptosis, cells were treated with different concentrations of 6c for 24 h, stained with Hoechst 33342, and observed under an inverted fluorescence microscope. The results of apoptosis measured by flow were consistent with the staining results of Hoechst 33342 observed by fluorescence microscopy. As shown in Figure 7A and B, compound 6c induced obvious morphological changes of apoptosis, including cell shrinkage and the formation of granular apoptotic bodies. In conclusion, compound 6c induces apoptosis in Huh7 cells.

Induction of Cell Cycle Block by Compound 6c

Previous studies have shown that artesunate can inhibit the proliferation of tumor cells by generating ROS to induce tumor cell cycle arrest.[28] In order to further study the specific mechanism of 6c's inhibitory effect on HCC proliferation and apoptosis, propidium iodide (PI) staining was used to detect the effect of cell cycle with the treatment of 6c. Different concentrations of 6c were incubated for 24 h in Huh7 cells. The result showed that 6c reduced G1/G0 phase cells from

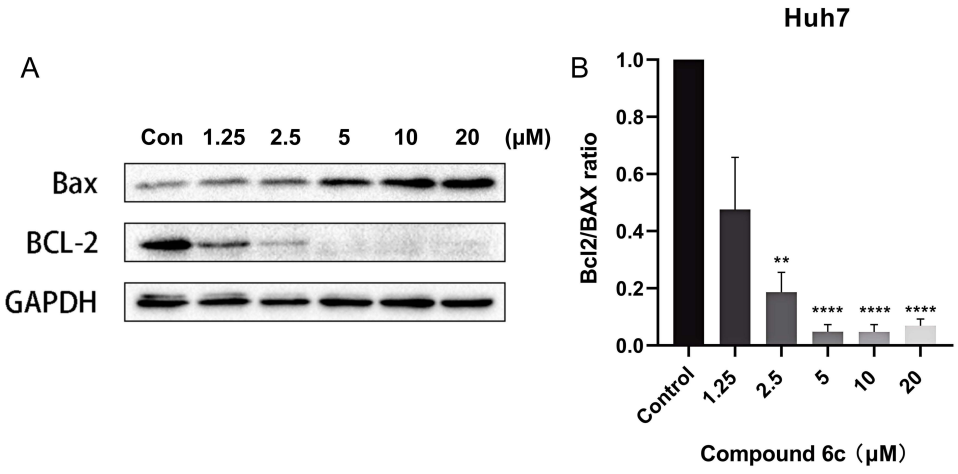

Figure 5 Compound 6c activates the mitochondrial apoptosis pathway. (**A**) Protein expression levels of Huh7 cells treated with different concentrations of 6c for 48 h in Western blot assay. (**B**) Summary from Bcl-2/Bax expression ratio from (**A**). **P <0.01; ****P <0.0001.
Abbreviations: ns, not significant.

48% to 38%, and S phase cells from 45% to 39%. However, there was a significant increase in the G2/M phase, from 6% to 22% (Figure 8A and B). These results indicate that compound 6c induces Huh7 cells cycle arrest in the G2/M phase.

Molecular Docking

Molecular simulation is considered to be an important tool to study the interaction of certain ligand molecules and the corresponding protein-binding sites. This series of hybrids consist of the artesunate moiety and the fragment of sorafenib, 4-(4-aminophenoxy)-n-methyl-2-pyridine, both of which are inhibitory to VEGFR-2 kinase. Therefore, as shown in Figure 9A–C, the representative hybrid 6c was used as the ligand for this docking analysis, and the MOE program was used to conduct a molecular docking study on the three-dimensional structure of VEGFR-2 (PDB:3IAI). The Molecular docking results showed that the artesunate part of compound 6c was in good agreement with the hydrophobic entrance of VEGFR-2 and the 4-(4-aminophenoxy)-n-methyl-2-pyridine fragment could interact with the active site of VEGFR-2. The cavities of the dots are tightly bound with a minimum binding energy of (ΔG) −8.2 kcal/mol. At the active site of VRGFR-2, compound 6c forms 3 hydrogen bonds with ARG-842, ARG-1051, and LYS-838. The artesunate moiety and the 4-(4-aminophenoxy)-N-methyl-2-pyridinecarboxamide fragment are both involved in the interaction. Next, we selected the compound 6a, 6d, 11d, and 11e, as ligands to conduct molecular docking studies on VEGFR-2 (PDB: 3IAI). The minimum binding energy of these hybrids is shown in Table 2. It can be seen from the results that 6a and 6c have the best match with the active region of VEGFR-2, while 6d, 11d, and 11e do not match well with the active region of VEGFR-2, so it can also explain why they have worse activity. Compared with artesunate, the binding ability of these hybrids to VEGFR-2 protein is significantly improved, and the minimum binding energies of 6a and 6c are similar to those of sorafenib, indicating that these two hybrids have excellent binding ability to VEGFR-2. The different activities of this series of hybrids may be due to the 4-(4-amino phenoxy) -N-Methyl-2-pyridinecarboxamide group and the artesunate group being connected by different lengths and connection positions. Combined with the results of cell activity studies, VEGFR-2 may be one of the drug targets of AS-4-(4-aminophenoxy) -N-methyl-2-pyridinecarboxamide hybrids.

Secondly, we have confirmed that these hybrids could induce intracellular ROS level increased, it recommends 6c and other derivates participate in the ROS generation cascade pathway. TFR1 (Transferrin receptor protein 1), a type II transmembrane protein, is a crucial membrane protein that regulates the intracellular transport of iron. Under environment homeostasis, TFR1 interacts with transferrin Tf to promote iron absorption. This binding form is the main form of iron present in the plasma. TFR1 is a direct target of AS, and AS can improve intracellular ROS levels via moderating TFR1 expression.[29]

https://doi.org/10.2147/JHC.S490445

https://doi.org/10.2147/JHC.S490445

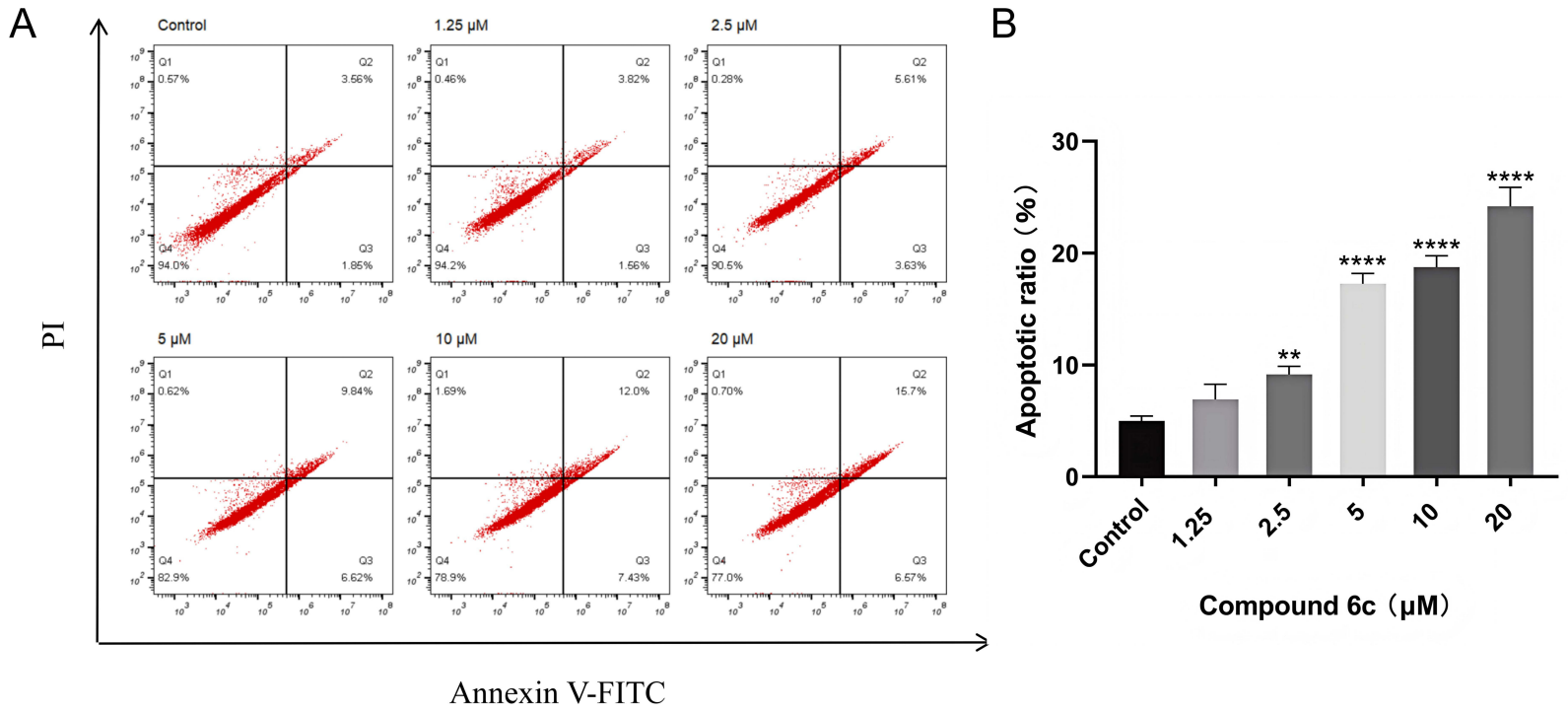

Figure 6 Induction of apoptosis in Huh7 cells by compound 6c. (**A**) Cells were treated with different concentrations of 6c for 24h. Cells were collected and washed with PBS, incubated with Annexin-FITC and PI in binding buffer, and at final detected by FACS. (**B**) Summary of FACS analysis for ratio of apoptosis from (**A**). ***P* <0.01; *****P* <0.0001.
Abbreviations: ns, not significant.

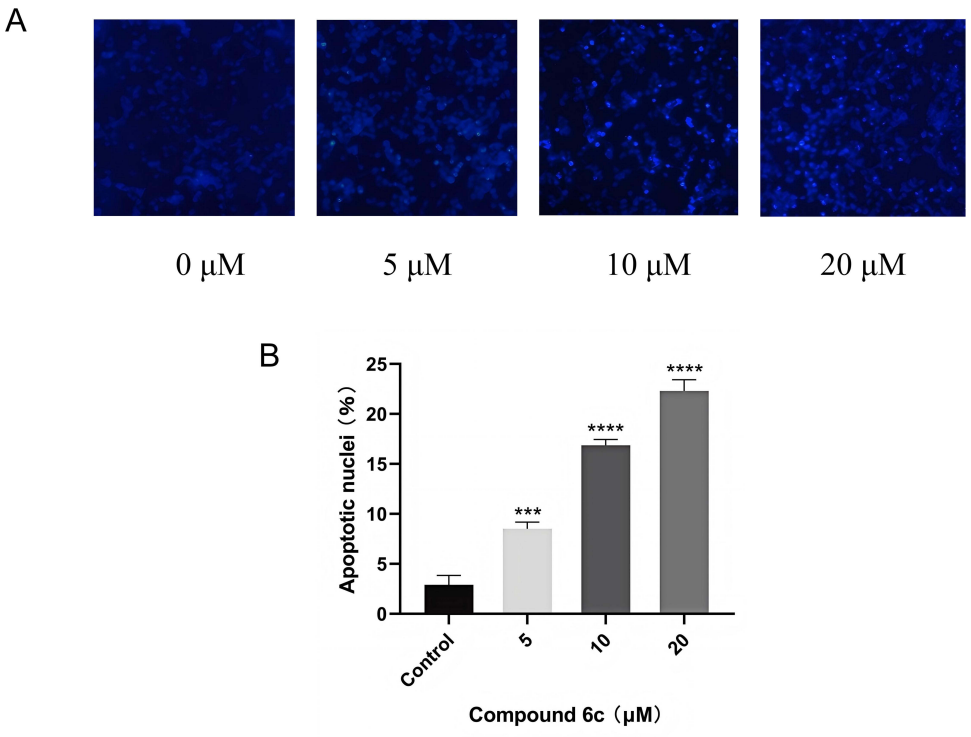

Figure 7 The introduction of cell apoptosis morphological changes in Huh7 cells by compound 6c. (**A**) Cells were treated with different concentrations of compound 6c, and then incubated with Hoechst 33342, and finally detected by fluorescence microscope. (**B**) Summary of fluorescent analysis for apoptosis ratio from (**A**). ***P <0.001; ****P <0.0001.

Abbreviations: ns, not significant.

Hence, we used some hybrids to dock with TFR1 (Figure 9D–F). It can be seen that 6a and 6c have the best match scores with the active region of TRF1 than 6d, 11d, and 11e (Table 2). All of these hybrids show better match scores than AS and Sorafenib, this result recommends that these new compounds may work through the TRFC/Fe^{2+} pathway. According to the molecular interacting diagram, 6c can knob into the hole of TFR1, forming 4 hydrogen bonds with ARG-174, VAL-181, LYS-177, and GLU-175.

In vivo Antitumor Activity

Finally, we tested the anti-HCC efficacy of 6c in Huh7 cells mouse xenograft model. Sorafenib, artesunate, and 6c were administered in female BALB-c nude mice. 6c shows strong tumor inhibition effect than control group, 10 mg/kg compound 6c treatment were used in test, 100 mg/kg artesunate and 10 mg/kg sorafenib treatment were used as control (Figure 10A). Meanwhile, no obvious change in body weight were observed in this procedure (Figure 10B). It indicated that compound 6c is safety. These results demonstrated that 6c have promising anti-HCC capability.

Discussion

Currently, drug resistance and severe side effects are the main problems in the first-line treatment of hepatocellular carcinoma.[30] Artesunate, which has moderate anti-cancer activity and low toxicity, seems to be a perfect solution to this problem. However, the anti-HCC activity of artesunate is not ideal, and they have poor selectivity for HCC, so its anti-HCC efficacy needs to be significantly improved. Therefore, the structure of artesunate needs to be modified to improve anti-HCC activity and retain low toxicity to normal cells so as to find promising new anti-HCC cancer candidate drugs. So far, there is little relevant research in this field. This work used artesunate as the structural core and molecular hybridization technology was used to assemble the 4-(4-substituted phenoxy) pyridine moiety. The biological activities of 6a, 6b, 6c, and 11c in three HCC cell lines are better than or similar to sorafenib and partially retain the low toxicity

https://doi.org/10.2147/JHC.S490445

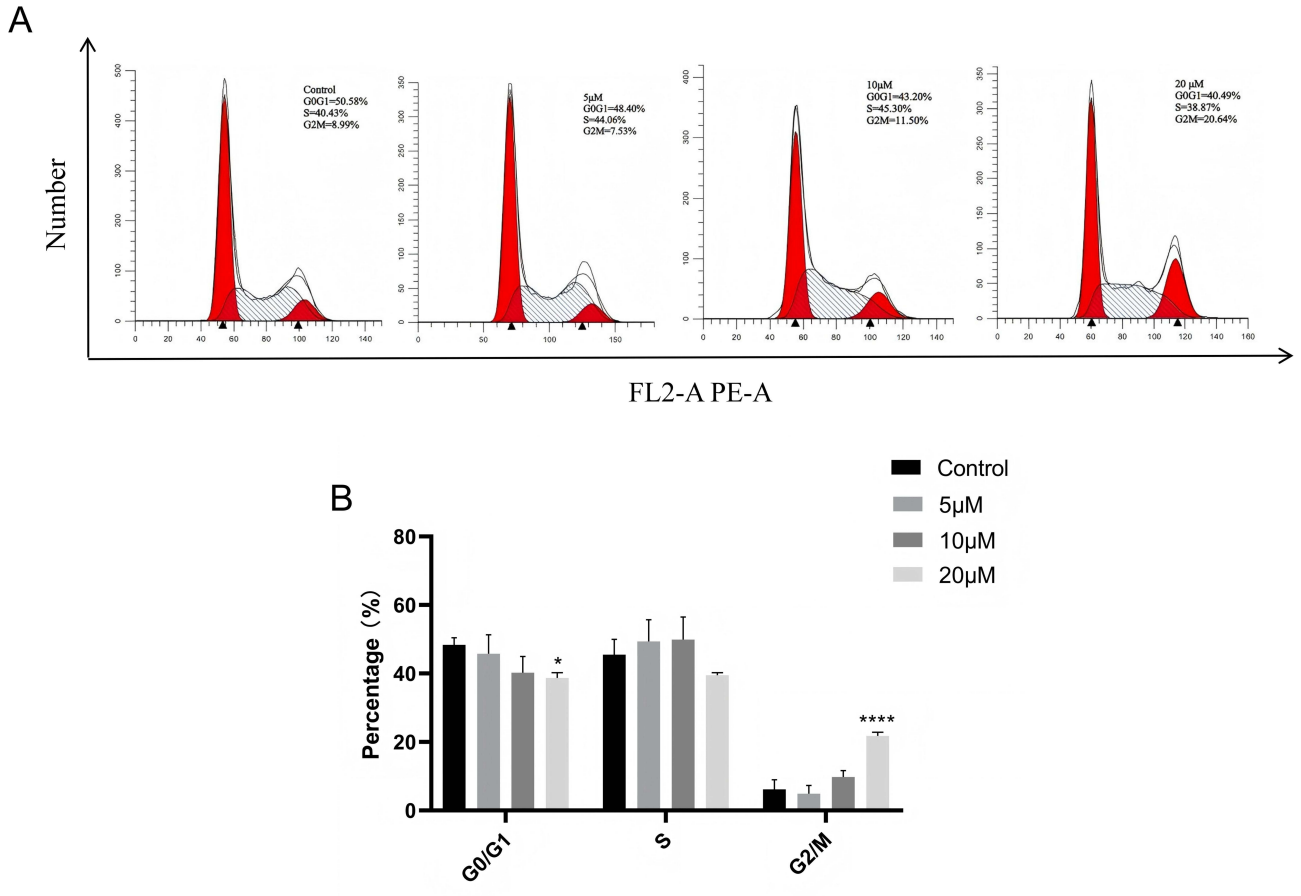

Figure 8 Induction of G2/ M-phase cell cycle arrest in Huh7 cells by compound 6c. (**A**) Cells were treated with different concentrations of compound 6c for 24 hours and then treated with 0.25% trypsin. Cells were collected and washed with PBS, incubated with PI, and finally detected by FACS in flow cytometry. (**B**) Summary of FACS analysis for the ratio of cell cycle from (**A**). **P* <0.05; *****P* <0.0001.
Abbreviations: ns, not significant.

properties. In particular, cytotoxicity of compound 6c was 12 times lower than that of sorafenib in normal human liver cells. Ren et al reported several promising artesunate derivatives, such as 3e and 3f, whose IC_{50} in HepG2 cells were 8.85 μM and 8.38 μM, respectively, and their IC_{50} in human normal liver cells LO2 were more than 50 μM.[31] Awasthi et al reported that sorafenib derivatives 4 and 6 had IC_{50} of 5.29 μM and 4.77 μM in Huh7 cells, respectively, and their IC_{50} in H6c7 cells (human normal pancreatic duct epithelial cells) and CCD841 cells (human normal colon epithelial cells) were more than 10 μM.[32] Sbenati et al reported that sorafenib derivative 1h had IC_{50} of 4.31 μM in Huh7 cells, and its IC_{50} in WI-38 cells (human embryonic lung fibroblasts) was more than 30 μM.[33] Our compound 6c had an IC_{50} of 8.5 μM in HepG2 cells and an IC_{50} of 2.25 μM in Huh7 cells, and its IC_{50} in LO2 cells (human normal liver cells) was more than 100 μM. Compared with them, the safety of compound 6c has more significant potential.

We conducted biological and functional evaluations on compound 6c with a high selectivity index. Through MTT experiments, we found that compound 6c can inhibit the proliferation of HCC in a time- and concentration-dependent manner. Due to the unique peroxide bridge structure of artesunate, the detection experiment of ROS level proved that 6c induced Huh7 and Hep3B cells to produce ROS in a concentration-dependent manner. After adding the ROS inhibitor NAC, the inhibition of Huh7 and Hep3B cells induced by 6c was reversed in a time- and concentration-dependent manner, indicating that 6c exerts its anti-HCC effect by regulating intracellular ROS. According to previous studies, reactive oxygen species are a double-edged sword. Low levels of reactive oxygen species promote cell proliferation, while high levels of reactive oxygen species accumulation can lead to cell apoptosis, necrosis, and ferroptosis. Western blot results showed that 6c activated the mitochondrial apoptosis pathway, increased the expression of Bax, and reduced

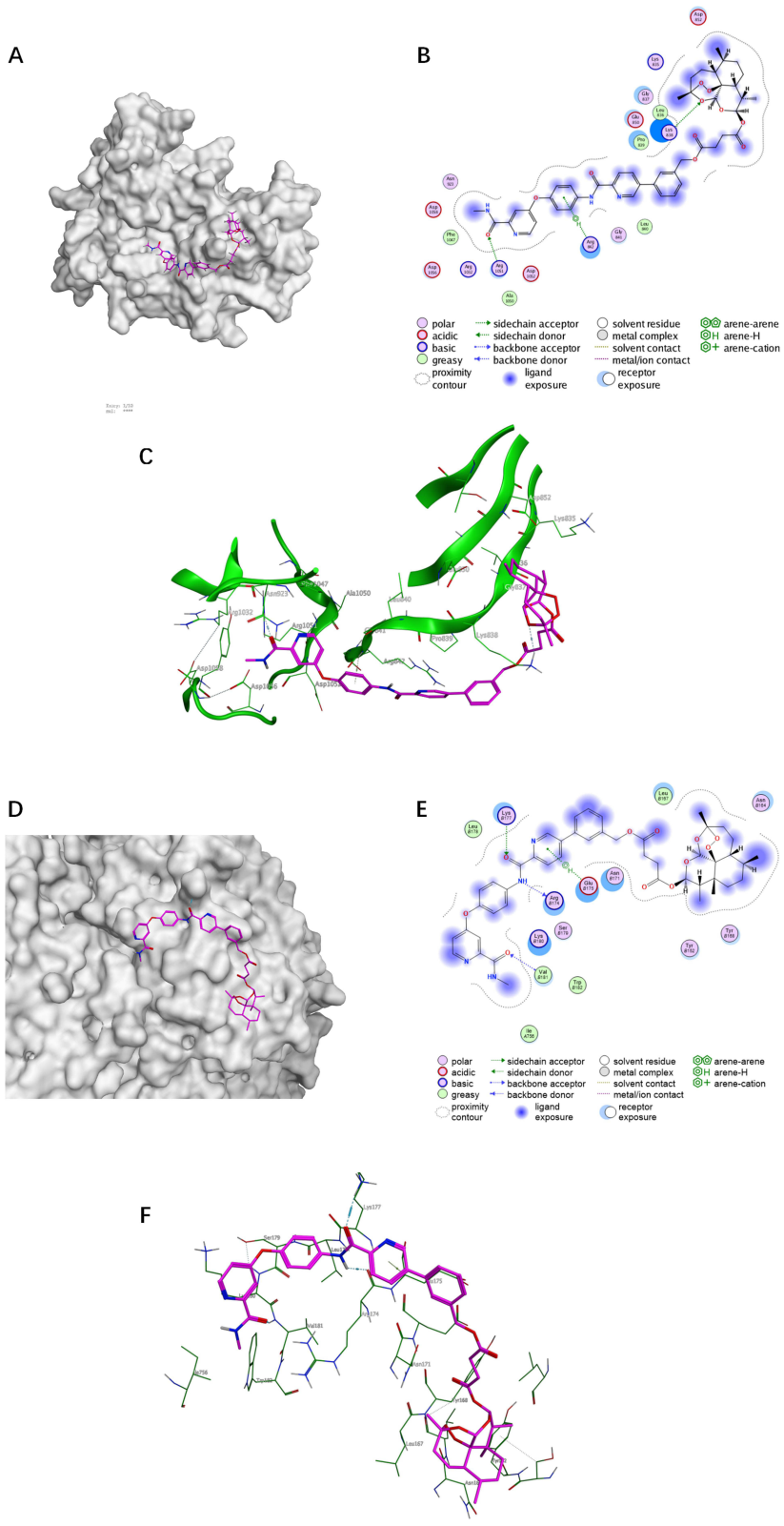

Figure 9 Interaction diagrams of the selected docked conformations for compound 6c inside the active site of *VEGFR-2* and *TFR1*. (**A**) The surface representation of the binding pocket of *VEGFR-2*. (**B**) 2D ligand interactions diagram of *VEGFR-2*. (**C**) 3D ligand interactions diagram of *VEGFR-2*. (**D**) The surface representation of the binding pocket of *TFR1*. (**E**) 2D ligand interactions diagram of *TFR1*. (**F**) 3D ligand interactions diagram of *TFR1*.

https://doi.org/10.2147/JHC.S490445

Table 2 Minimum Free Energy for Docking of Compounds with Targets

Compound	VEGFR2/ΔG (kcal/mol)	TFRC/ΔG (kcal/mol)
Sora	−8.1	−6.9
AS	−6.5	−5.9
6a	−8.2	−8.9
6c	−8.2	−8.7
6d	−8.1	−7.8
11d	−7.8	−7.9
11e	−7.3	−8.3

the expression of Bcl-2. The results of the PI/Annexin V-FITC double staining experiment showed that 6c induced Huh7 cell apoptosis in a concentration-dependent manner. In the Hoechst 33342 staining experiment, morphological changes were observed in Huh7 cells caused by 6c, which further verified that 6c can induce apoptosis of HCC. The above results indicate that 6c can activate the mitochondrial-induced apoptosis pathway in a reactive oxygen species-dependent manner. Then, by adding Liproxstatin-1 (ferroptosis inhibitor), it was found that Liproxstatin-1 reversed the inhibition of Huh7 cells induced by 6c in a time- and concentration-dependent manner, indicating that 6c can induce ferroptosis in Huh7 cells by producing reactive oxygen species. The results of the cycle detection by PI staining showed that 6c blocked the cell cycle progression of Huh7 cells and kept them in the G2/M phase. Molecular docking results proved that VEGFR2 and TFRC are the potential targets of 6c, but further experimental confirmation is needed. Finally, the xenograft tumor model confirmed the significant activity of 6c in vivo. Therefore, we preliminarily elucidated the anti-HCC mechanism of compound 6c (Figure 11). In general, as a new type of anti-HCC lead drug, 6c has a promising research background in the future.

While some of these compounds using artesunate as the structural core have achieved strong biological activity similar to sorafenib, the results have not yet reached the desired nanomolar levels. This problem may be attributed to the high polarity and large molecular weight of these compounds, which hinder their ability to penetrate cell membranes and result in insufficient binding rates with target proteins. Meanwhile, safety has been confirmed in the cellular, but there is a lack of research on animals. In subsequent experimental studies, we will conduct more in-depth research on 6c, such as pharmacokinetics, tissue distribution, safety pharmacology, and toxicology.

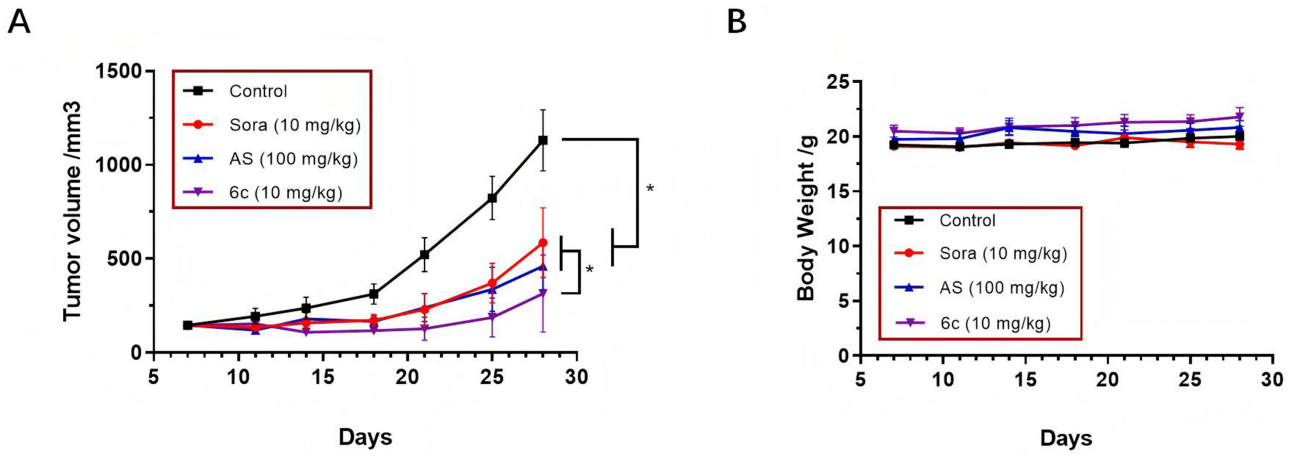

Figure 10 In vivo anti-HCC efficacy of 6c in Huh7 cells mouse xenograft model. Female BALB/c nude mouse were treated by 100 mg/kg artesunate, 10 mg/kg sorafenib, and 10 mg/kg compound 6c via intraperitoneal injection for 21 days (n=5). (**A**) Tumor volume of mouse was measured twice a week. (**B**) Body weight of mouse was measured twice a week. *P <0.05.
Abbreviations: ns, not significant.

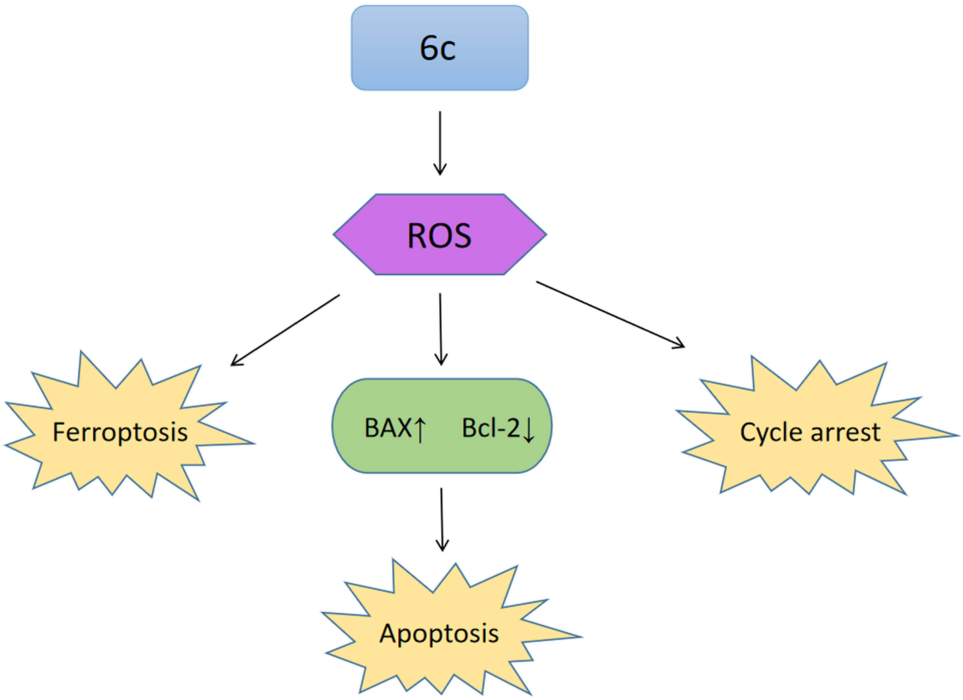

Figure 11 Proposed mechanism of action of 6c.

Conclusions

Novel artesunate hybrids were designed and synthesized by hybridization of AS and 4-(4-substituted phenoxy) pyridine pharmacophore via different types of linkers. Among these hybrids, compound 6c shows robust anti-proliferative activity against HepG2, Hep3B, Huh7 cells lines with significant improvement against the anti-tumor growth than lead compound. Although the IC_{50} of 6c against three HCC cell lines is equivalent to sorafenib, its IC_{50} against normal liver cells is much higher than sorafenib. Meanwhile, 6c shows excellent anti-HCC activity in Huh7 cells mouse xenograft model. This promising result indicates that compound 6c provides a new structural lead for the development of new anti-HCC tumor drugs.

Mechanistically, 6c induces HCC cells ferroptosis and apoptosis through reactive oxygen species and reduction of Bcl-2/Bax ratio, preventing the cell cycle process of HCC cells to stay in the G2/M phase. 6c acquires better match scores than lead compound AS in Docking with TFR1 and VEGFR2, it indicates that TFR1 and VEGFR2 may be the direct targets of 6c. Overall, compound 6c hold developmental potential for therapy of anti-HCC.

Experimental Section

Chemical Synthesis

All commercial reagents (Bide, Macklin, Aladin, China) were purchased with a purity above 95%. All reactions were carried out under nitrogen atmosphere. All reaction products were purified by silica gel column chromatography.

General Procedure for Preparation of Intermediate 3

Details are in the Supplementary (Figure S2).

General Procedure for Preparation of Intermediates 5a-5e

Details are in the Supplementary (Figures S3–S7).

General Procedure for Preparation of Hybrids 6a-6e

Details are in the Supplementary (Figures S8–S12).

https://doi.org/10.2147/JHC.S490445

General Procedure for Preparation of Intermediate 9

Details are in the Supplementary (Figure S13).

General Procedure for Preparation of Intermediates 10a-10e

Details are in the Supplementary (Figures S14–S18).

General Procedure for Preparation of Hybrids 11a-11e

Details are in the Supplementary (Figures S19–S23).

General Procedure for Preparation of Hybrid 12

Details are in the Supplementary (Figure S24).

Biological Assay

Cell Culture

HCC cell lines, including Huh7, HepG2, and Hep3B, and normal human hepatocytes LO2 were obtained from the National Infrastructure of Cell Line Resource (Beijing, China). Huh7, HepG2, and LO2 cells were cultured in Dulbecco's modified Eagle's medium (DMEM, Gibco, USA) supplemented with 10% fetal bovine serum (Hyclone, Australia). Hep3B cells were cultured in modified Eagle's medium (MEM, Gibco, USA) supplemented with 10% fetal bovine serum (Hyclone, Australia).

Cell Viability Assay

Cell viability assay was measured using 3-(4,5-dimethyl-2-thiazolyl)-2,5-diphenyl-2-H-tetrazolium bromide (MTT, Aladdin, China) assay. The cytotoxicity of compounds was tested in Hep3B, Huh7, HepG2, and LO2 cells. 5×10^3 cells were plated in 96-well plates per well. After incubated overnight, old medium was discarded, and cells were treated with all compounds at 0.1, 0.3, 1, 3, 10, 30, and 100 μM for 24, 48, and 72h. Then, 0.5 mg/mL of MTT 50μL was added to each well and incubated for 4 h. The solution was removed, and 150 μM dimethyl sulfoxide was added to each well. Finally, we measured the absorbance on microplate reader (Gen5, BioTek).

ROS Level Detection

Huh7 and Hep3B cells were plated in 96-well plates at a density of 5×10^3 per well. After incubated overnight, old medium was discarded and cells were treated with 6c at 5, 10, 20 μM and incubated for 4 h. 1 μM DCFH-DA solution were added and incubated at RT for 20 min in the dark. Fluorescence intensity was measured at 480 nm after washing thrice with PBS.

Cell Cycle Analysis

Huh7 cells were plated in six-well plates at a density of 1.5×10^5 cells per well and incubated overnight. Old medium was discarded and cells were treated with 5 μM, 10 μM and 20 μM of compound 6c for 24 h. Then cells were digested, washed thrice with PBS and resuspended in PBS. The cooled 75% ethanol at 4°C was added to fix the cells overnight. The cells were concentrated by centrifugation and resuspended in PBS. Next, RNase A and Triton X-100 were added and incubated at 37°C for 30 min. Finally, propidium iodide was added and the mixture was incubated for 10 min. Cell cycle analysis was evaluated via PI fluorescence and flow cytometry (BD Accuri, C6). For each measurement, at least 10,000 cells were counted.

Cell Apoptosis Assay

Huh7 cells were plated in six-well plates at a density of 1.5×10^5 cells per well and incubated overnight. Old medium was discarded and cells were treated with 1.25 μM, 2.5 μM, 5μM, 10 μM and 20 μM of 6c for 24 h. Cells were then digested and washed thrice with PBS. After resuspending cells with binding buffer, add Annexin V-FITC/PI and incubate at RT for 15 min. Apoptotic cells were estimated in a flow cytometer (BD Accuri, C6). For each measurement, at least 10,000 cells were counted.

Hoechst 33342 Staining

Huh7 cells were plated in six-well plates at a density of 1.5×10^5 cells per well and incubated overnight. Old medium was discarded, and cells were treated with 5 μM, 10 μM and 20 μM of 6c for 24 h. Add Hoechst 33342 staining solution and incubate at RT for 30 min. Fluorescence detection was performed after washing twice with PBS.

Western Blot

Huh7 cells were plated (1.5×10^5 cells/well) in six-well plates and incubated overnight. The cells were treated with 1.25 μM, 2.5 μM, 5 μM and 10 μM, 20 μM of 6c for 48 h. Whole cells (attached and floating cells) were extracted with cell lysis buffer and were boiled for 5 min at 95°C. The resultant proteins were separated using 12% SDS-PAGE and transferred to PVDF membrane at 100 V for 45 min. After washing with TBST (0.1% Tween-20, TBS) for 5 min, the membrane was blocked for 90 min at RT in blocking buffer (5% skim milk, 0.1% Tween-20, TBS) and then incubated with primary antibody in blocking buffer at 4°C overnight. The blot was then washed with TBST three times for 5 min and incubated with secondary antibody in blocking buffer for 1 h at RT. After being washed with TBST, the blot was analyzed with the ECL Western blot detection system (Sigma, USA).

Molecular Docking

We obtained the experimental crystal structure of the VEGFR-2 complex (Protein ID: 3IAI) and TFR1 complex (Protein ID: 2NSU) from Protein Data Bank. The molecular model of ligand was built by Chem3D. The protein's water molecules and ligands are removed, and polar hydrogen atoms and partial charges are added on MOE (CCG). The energy of the drug is then minimized. Using the all-atom docking method, the docked ligands will keep attacking the pockets on the protein surface until the most stable docking complex is reached. Scoring energy is the average of trials using the London ΔdG scoring function, upgraded with two uncorrelated refinements by the triangle Matcher method. Finally, the 2D interact diagram, 3D interact diagram, and pocket diagram of the ligand-protein docking are obtained. All other parameters are set to default unless otherwise specified.

Antitumor Activity Evaluation in vivo

Female BALB/c nude mice at 5 weeks of age, weighing between 16 g and 20 g were purchased (Vital River; Beijing). 5.0×10^6 tumor cells to be inoculated were suspended in 0.1 mL PBS and inoculated into the right scapula of nude mice (P1). When the tumor grew to 500–800 mm^3, the tumor-bearing mice were killed with CO_2, the surrounding necrotic tissue was removed, and the tumor in good condition was cut into small size of 20–30 mm^3 and inoculated into the right scapula of a new batch of nude mice (P2). 7 days after tumor inoculation, when the average tumor volume reached about 150 mm^3, mice with tumors that were too small or too large were eliminated, and the remaining mice were randomly divided into groups according to tumor volume and began to be administrated.

Statistical Analysis

The experimental results are presented as the mean ± standard deviation (SD) or standard error of mean (SEM) of experiments repeated at least three times. For each significant treatment effect, ANOVA or *t*-test was used to compare the multiple group's means. The criterion for statistical significance was set as $*P<0.05$, $**P<0.01$, $***P<0.001$, $****P<0.0001$.

Abbreviations

AS, artesunate; Sora, sorafenib; HCC, Hepatocellular carcinoma; ROS, reactive oxygen species; DMAP, 4-Dimethylaminopyridine; EDCL, 1-Ethyl-3-(3-dimethylaminopropyl) carbodiimide hydrochloride; NAC, N-acetylcysteine; PI, propidium iodide, MTT, 3-(4,5-dimethyl-2-thiazolyl)-2,5-diphenyl-2-H-tetrazoli um bromide.

Ethics Approval

The study was approved by the Ethics Committee for Laboratory Animal Management of Suzhou Weiyuan Biotechnology Co., Ltd. (NO.20240313) and conformed to the Guide for the Care and Use of Laboratory Animals prepared by AAALAC international and the Ministry of Science and Technology of China.

Acknowledgments

S. S. Xiong designed, performed, and analyzed the data for the experiment and drafted the manuscript. We would like to thank the School of Pharmacy of Qingdao University and Suzhou Weiyuan Biotechnology Co., Ltd. for providing laboratory and SPF-class experimental animal room.

Funding

The study was supported by Innovative drug Research Institute of Qingdao University (Grant No. 2019021017).

Disclosure

The author declares there is no conflict of interest.

References

1. Bray F, Laversanne M, Sung H, et al. Global cancer statistics 2022: GLOBOCAN estimates of incidence and mortality worldwide for 36 cancers in 185 countries. *CA Cancer J Clin*. 2024;74(3):229–263. doi:10.3322/caac.21834
2. Llovet JM, Montal R, Sia D, Finn RS. Molecular therapies and precision medicine for hepatocellular carcinoma. *Nat Rev Clin Oncol*. 2018;15(10):599–616. doi:10.1038/s41571-018-0073-4
3. Klayman DL. Qinghaosu (artemisinin): an antimalarial drug from China. *Science*. 1985;228(4703):1049–1055. doi:10.1126/science.3887571
4. WHO Guidelines Approved by the Guidelines Review Committee. *Guidelines for the Treatment of Malaria*. World Health Organization; 2015.
5. Newton P, Suputtamongkol Y, Teja-Isavadharm P, et al. Antimalarial bioavailability and disposition of artesunate in acute falciparum malaria. *Antimicrob Agents Chemother*. 2000;44(4):972–977. doi:10.1128/aac.44.4.972-977.2000
6. Blazquez AG, Fernandez-Dolon M, Sanchez-Vicente L, et al. Novel artemisinin derivatives with potential usefulness against liver/colon cancer and viral hepatitis. *Bioorg Med Chem*. 2013;21(14):4432–4441. doi:10.1016/j.bmc.2013.04.059
7. Ma Z, Woon CY, Liu CG, et al. Repurposing artemisinin and its derivatives as anticancer drugs: a chance or challenge? *Front Pharmacol*. 2021;12:828856. doi:10.3389/fphar.2021.828856
8. Peter S, Jama S, Alven S, Aderibigbe BA. Artemisinin and derivatives-based hybrid compounds: promising therapeutics for the treatment of cancer and malaria. *Molecules*. 2021;26(24):7521. doi:10.3390/molecules26247521
9. Zou X, Liu C, Li C, et al. Study on the structure-activity relationship of dihydroartemisinin derivatives: discovery, synthesis, and biological evaluation of dihydroartemisinin-bile acid conjugates as potential anticancer agents. *Eur J Med Chem*. 2021;225:113754. doi:10.1016/j.ejmech.2021.113754
10. Tiwari MK, Coghi P, Agrawal P, et al. Novel halogenated arylvinyl-1,2,4 trioxanes as potent antiplasmodial as well as anticancer agents: synthesis, bioevaluation, structure-activity relationship and in-silico studies. *Eur J Med Chem*. 2021;224:113685. doi:10.1016/j.ejmech.2021.113685
11. Meunier B, Robert A. Heme as trigger and target for trioxane-containing antimalarial drugs. *Acc Chem Res*. 2010;43(11):1444–1451. doi:10.1021/ar100070k
12. Posner GH, O'Neill PM. Knowledge of the proposed chemical mechanism of action and cytochrome P450 metabolism of antimalarial trioxanes like artemisinin allows rational design of new antimalarial peroxides. *Acc Chem Res*. 2004;37(6):397–404. doi:10.1021/ar020227u
13. Lu YY, Chen TS, Wang XP, Li L. Single-cell analysis of dihydroartemisinin-induced apoptosis through reactive oxygen species-mediated caspase-8 activation and mitochondrial pathway in ASTC-A-1 cells using fluorescence imaging techniques. *J Biomed Opt*. 2010;15(4):16.046028. doi:10.1117/1.3481141
14. Stockwin LH, Han B, Yu SX, et al. Artemisinin dimer anticancer activity correlates with heme-catalyzed reactive oxygen species generation and endoplasmic reticulum stress induction. *Int J Cancer*. 2009;125(6):1266–1275. doi:10.1002/ijc.24496
15. Zhou XJ, Chen Y, Wang FF, et al. Artesunate induces autophagy dependent apoptosis through upregulating ROS and activating AMPK-mTOR-ULK1 axis in human bladder cancer cells. *Chem Biol Interact*. 2020;331:109273. doi:10.1016/j.cbi.2020.109273
16. Ji P, Huang HQ, Yuan SR, et al. ROS-mediated apoptosis and anticancer effect achieved by artesunate and auxiliary Fe(II) released from ferriferous oxide-containing recombinant apoferritin. *Adv Healthc Mater*. 2019;8(23):1900911. doi:10.1002/adhm.201900911
17. Pang YL, Qin GQ, Wu LP, Wang XP, Chen TS. Artesunate induces ROS-dependent apoptosis via a Bax-mediated intrinsic pathway in Huh-7 and Hep3B cells. *Exp Cell Res*. 2016;347(2):251–260. doi:10.1016/j.yexcr.2016.06.012
18. Song QX, Peng SX, Che FY, Zhu XS. Artesunate induces ferroptosis via modulation of p38 and ERK signaling pathway in glioblastoma cells. *J Pharmacol Sci*. 2022;148(3):300–306. doi:10.1016/j.jphs.2022.01.007
19. Wang LL, Kong L, Liu H, et al. Design and synthesis of novel artemisinin derivatives with potent activities against colorectal cancer in vitro and in vivo. *Eur J Med Chem*. 2019;182:111665. doi:10.1016/j.ejmech.2019.111665
20. Luan S, Zhong H, Zhao X, et al. Synthesis, anticancer evaluation and pharmacokinetic study of novel 10-O-phenyl ethers of dihydroartemisinin. *Eur J Med Chem*. 2017;141:584–595. doi:10.1016/j.ejmech.2017.10.023
21. Yu H, Hou Z, Tian Y, Mou Y, Guo C. Design, synthesis, cytotoxicity and mechanism of novel dihydroartemisinin-coumarin hybrids as potential anti-cancer agents. *Eur J Med Chem*. 2018;151:434–449. doi:10.1016/j.ejmech.2018.04.005
22. Ding L, Pannecouque C, De Clercq E, Zhuang C, Chen F-E. Discovery of novel pyridine-dimethyl-phenyl-DAPY hybrids by molecular fusing of methyl-pyrimidine-DAPYs and difluoro-pyridinyl-DAPYs: improving the druggability toward high inhibitory activity, solubility, safety, and PK. *J Med Chem*. 2022;65(3):2122–2138. doi:10.1021/acs.jmedchem.1c01676
23. Yao X, Zhao CR, Yin H, Wang KW, Gao JJ. Synergistic antitumor activity of sorafenib and artesunate in hepatocellular carcinoma cells. *Acta Pharmacol Sin*. 2020;41(12):1609–1620. doi:10.1038/s41401-020-0395-5
24. He WB, Huang XX, Berges BK, et al. Artesunate regulates neurite outgrowth inhibitor protein B receptor to overcome resistance to Sorafenib in hepatocellular carcinoma cells. *Front Pharmacol*. 2021;12:9.615889. doi:10.3389/fphar.2021.615889

25. Li ZJ, Dai HQ, Huang XW, et al. Artesunate synergizes with sorafenib to induce ferroptosis in hepatocellular carcinoma. *Acta Pharmacol Sin*. 2021;42(2):301–310. doi:10.1038/s41401-020-0478-3
26. Park E, Chung SW. ROS-mediated autophagy increases intracellular iron levels and ferroptosis by ferritin and transferrin receptor regulation. *Cell Death Dis*. 2019;10:10.822. doi:10.1038/s41419-019-2064-5
27. Guo L, Yang Y, Sheng YJ, Wang J, Ruan SL, Han CY. Mechanism of piperine in affecting apoptosis and proliferation of gastric cancer cells via ROS-mitochondria-associated signalling pathway. *J Cell Mol Med*. 2021;25(20):9513–9522. doi:10.1111/jcmm.16891
28. Du X, Fu XF, Yao K, et al. Bcl-2 delays cell cycle through mitochondrial ATP and ROS. *Cell Cycle*. 2017;16(7):707–713. doi:10.1080/15384101.2017.1295182
29. Liu Y, Li H, Luo Z, et al. Artesunate, a new antimalarial clinical drug, exhibits potent anti-AML activity by targeting the ROS/Bim and TFRC/Fe(2+) pathways. *Br J Pharmacol*. 2023;180(6):701–720. doi:10.1111/bph.15986
30. Alawyia B, Constantinou C. Hepatocellular carcinoma: a narrative review on current knowledge and future prospects. *Curr Treat Options Oncol*. 2023;24(7):711–724. doi:10.1007/s11864-023-01098-9
31. Ren M, Liang S, Lin S, et al. Design, synthesis and biological evaluation of artesunate-Se derivatives as anticancer agents by inducing GPX4-mediated ferroptosis. *Bioorg Chem*. 2024;152:107733. doi:10.1016/j.bioorg.2024.107733
32. Awasthi BP, Chaudhary P, Guragain D, Jee JG, Kim JA, Jeong BS. Synthesis and anti-hepatocellular carcinoma activity of aminopyridinol-sorafenib hybrids. *J Enzyme Inhib Med Chem*. 2021;36(1):1884–1897. doi:10.1080/14756366.2021.1953997
33. Sbenati RM, Zaraei SO, El-Gamal MI, et al. Design, synthesis, biological evaluation, and modeling studies of novel conformationally-restricted analogues of sorafenib as selective kinase-inhibitory antiproliferative agents against hepatocellular carcinoma cells. *Eur J Med Chem*. 2021;210:113081. doi:10.1016/j.ejmech.2020.113081